Atom Indonesia

Journal homepage: https://atomindonesia.brin.go.id

Development of a Vietnamese PET/CT Dataset for Machine Learning-Based Analysis of Non-Small Cell Lung Cancer Images

H. Q. Tuan[1], T. T. Duong[2*], B. N. Ha[2], N. H. Quyet[1], L. V. Tinh[3], C. V. Tuynh[4], V. K. Nam[5], L. T. Q. Dao[5], C. V. Luong[3], D. T. M. Linh[1], D. T. Nhung[1], N. D. Nguyen[1], V. Q. Trang[6]

[1]*Vietnam Atomic Energy Institute, No 59 Ly Thuong Kiet, Hanoi 11019, Vietnam*
[2]*Hanoi University of Science and Technology, No 1 Dai Co Viet, Hanoi 11615, Vietnam*
[3]*Vietnam National Cancer Hospital, No.30 Cau Buou St., Tan Trieu Commue, Thanh Tri district, Hanoi 12511, Vietnam*
[4]*Hanoi Oncology Hospital, No.42A Thanh Nhan, Thanh Nhan ward, Hai Ba Trung district, Hanoi 11624, Vietnam*
[5]*Oncology Hospital, No.12 D400, Long Thanh My St., 9 district, Ho Chi Minh city 71216, Vietnam*
[6]*National Hospital of Endocrinology, Nguyen Bo St. Thanh Tri district, Hanoi 12508, Vietnam*

ARTICLE INFO

Article history:
Received 4 March 2025
Received in revised form 4 May 2025
Accepted 8 May 2025

Keywords:
Radiology
Nuclear medicine
PET/CT
Lung cancer
Machine learning

ABSTRACT

Positron Emission Tomography and Computed Tomography (PET/CT), a key imaging modality in nuclear medicine, Combines Anatomical (CT) and functional (PET) data for cancer diagnosis. Despite advancements in machine learning for automated medical image analysis, publicly available PET/CT datasets remain scarce, limiting Artificial Intelligence (AI) research compared to CT and MRI. This study built a publicly accessible PET/CT Vietnamese dataset for Non-Small Cell Lung Cancer (NSCLC). A total of 416 PET/CT scans were collected from three Vietnamese hospitals, including 300 NSCLC cases. Malignant FDG-sensitive lesions, identified via clinical PET/CT reports, were manually segmented in 3D (slice-by-slice) on PET images and validated by three experienced radiologists. The dataset includes both original and annotated DICOM files, along with clinical patient data. It achieved a dice similarity coefficient of 80.3 % and volume similarity of 81.9 %, demonstrating high segmentation accuracy comparable to other studies. This dataset supports AI-driven NSCLC research and contributes to global efforts in automated PET/CT analysis for nuclear medicine applications.

INTRODUCTION

Artificial Intelligence (AI) and Machine Learning (ML), specifically Deep Learning (DL), have been widely applied across various fields, enabling systems to operate more intelligently and efficiently. In certain scenarios, the image recognition capabilities of machines trained through DL can be better than humans, especially in tasks requiring rapid and accurate decision-making. Recently, the application of DL techniques for medical image segmentation has gained significant attention from scientists worldwide, owing to their ability to process and learn from large datasets with high accuracy and speed [1-5].

Lung cancer remains one of the most dangerous and fatal diseases worldwide. In recent years, the application of ML models to automatically classify and segment lung cancer on Positron Emission Tomography and Computed Tomography (PET/CT) images has gained increasing attention. For instance, a study on classifying mediastinal lymph nodes of non-small lung cancer cells from PET/CT images was published by Wang et al., (2017) [5]. The study used PET/CT data to trace lymph nodes from 168 patients and then employed various machine-learning models for classification.

*Corresponding author.
E-mail address: duongtran902@gmail.com
DOI: https://doi.org/10.55981/aij.2025.1645

The results showed that the Support Vector Machine (SVM) model achieved an accuracy of about 83 %, while the random forest, AdaBooost, and Convolutional Neural Network (CNN) models achieved about 85 %, and the Artificial Neural Network (ANN) model reached an accuracy of around 80 %. For comparison, the independent classification accuracy of the doctor was reprted at 81.61 % [5]. Furthermore, Zhao et al., (2018) [6] published a study on tumor segmentation from lung PET/CT images using the 3D CNN method. The study used PET/CT data from 84 patients to train the 3D CNN model. The results showed that the model achieved a Dice Similarity Coefficient (DSC) of 85 %, contrast-enhanced sensitivity of 33 %, and tumor volume deviation of 15 % [6]. Recently, the nnU-Net model was employed to automatically segment lung tumors from PET/CT images. The dataset included PET/CT scans from three groups of lung cancer patients, comprising 560 4D images for PET and 100 3D images for CT, all diagnosed by two independent experts. The model demonstrated high accuracy, with a DSC of 0.74 (4D) and 0.82 (3D) for PET images, and 0.61 (4D) and 0.63 (3D) for CT images, significantly outperforming manual segmentation. These models show strong potential for clinical practice by integrating biological and anatomical information from PET/CT scans, thereby reducing the time and workload required by physicians [7].

The data used for machine training plays a critical role in enabling algorithm development and training. In the process of developing an AI model, data is always the foundation. Across all AI research, classifying and labelling datasets often takes up the most time, especially data sets that are accurate enough to reflect reality [1-8]. Therefore, compiling high-quality image datasets is a crucial step in developing AI applications for medical image diagnosis. While many convolutional neural networks for image recognition require datasets with thousands of images, smaller datasets still hold significant value for tasks such as texture analysis, transfer learning, and programming. However, many commercial AI products rely on proprietary or institution-specific datasets that are inaccessible due to patient privacy restrictions. Some imaging datasets containing cancer images and/or reports are publicly available through platforms accessible to researchers, although they are often reside in PET oncology database. The Web-Based Diagnostic Imaging of Experts Network (wang) and the Cancer Imaging Archive (TCIA) are the two notable examples. Both platforms continue to grow through ongoing contributions and are expected to accelerate ML research in oncology [9,10].

The TCIA data repository as one of the best-known resources, offers a variety of curated image collections specifically focused on cancer imaging for use by various research institutions. All data in TCIA are completely de-identified using validated tools and procedures to comply with United States. and international privacy regulations. Although the number of online image repositories is increasing rapidly, few can match TCIA in supporting a wide variety of image data types, comprehensive metadata, robust data management processes, and versatile access methods for both human and computer. The rapid growth of research in machine learning-based quantitative image analysis has further expanded TCIA's mission to include providing datasets for training and testing new algorithms. This innitiative allows us to better understand the limitations imposed by existing data source on the development of novel machine learning models [9,10].

The Medical Imaging and Computer-Aided Intervention (MICCAI) conference has hosted several challenges on various medical imaging topics over the past few years. These challenges are organized by various institutions and provide the provision of curated datasets designed to address specific medical imaging problems. Such datasets often become standard benchmarks for evaluating new AI approaches, playing a crucial rolein ensuring reproducibility and enabling fair comparisons with state-of-the-art approaches. This practice facilitates more comprehensive evaluation, transparent replication, and clearer interpretation of challenge outcomes [11,12].

In studies exploring AI applications for diagnosing and segmenting PET-CT images, the patient cohort typically ranges from a few dozen to several hundred, aligning with the number of images analyzed. These studies incorporate datasets comprising a few thousand to hundreds of thousands of two-dimensional slice images, offering a substantial basis for developing and validating AI models. Multiple expert pathologists, specializing in lung tumors, meticulously reviewed the histological sections to ensure accurate annotations, thereby boosting the reliability of AI-driven results. The inclusion of such extensive imaging data and expert validation supports improved accuracy in detecting and classifying tumors.

Diagnostic results on CT images have lower sensitivity compared to PET/CT images, and false positive or misleading signs in CT scans can lead to misdiagnosis. It is difficult to determine the stage of the disease as accurately as PET/CT images. CT imaging primarily reveals the internal structure of the body, whereas PET imaging, through the uptake

of radiotracers suchas radioisotope absorption mechanism (FDG), provides functional information, pinpointing the exact location of tumors. Therefore, PET/CT data sets offer greater diagnostic significance than CT images.

Although databases such as TCIA or WIDEN do exist, the availability of PET/CT image data on lung cancer remains limited, and access to these datasets is often restricted. The small size of data sets and lack of diversity across different geographies can hinder the generalizability and accuracy of AI algorithms. While smaller data sets may suffice for algorithms development in research settings, large-scale data sets with high-quality images and detailed annotations are still essential for supervised training, validation, and testing commercial products.

This paper presents the process of collecting, processing, and evaluating PET/CT image data for lung cancer in Vietnam. This study aims to develop ML models capable of automatically classifying and segmenting PET/CT images, thereby assisting physicians in the diagnosis and treatment lung cancer.

METHODOLOGY

To achieve a high-quality imaging dataset, a multi-step data preparation process was implemented, following standardised protocols for medical imaging studies [8]. The process encompassed: (I) collecting images at clinical sites; (II) de-identifying images to remove personal information and protect patient privacy; (III) data management to control image information and quality; (IV) image storage and management; and finally (V) adding notes to and labelling images. The subsequent sections outline some key tasks required to build the dataset.

Selection criteria for patient data

Patient data were collected as part of a retrospective study, adhering to established guidelines for oncological imaging research [13]. The inclusion criteria for selecting patient imaging data were defined as follows: Y1- All patients were examined under the same imaging conditions and a consistent process using a standardised PET/CT protocol [14]; Y2- All selected cases were accompanied by pathological confirmation from surgical or biopsy specimens [15]; Y3- Each patient's dataset included a complete set of imaging data and comprehensive medical history [14].

Patients were excluded based on the following criteria: N1: Individuals with lung adenocarcinoma who had received radiation, chemotherapy, or targeted therapy prior to PET/CT examination were excluded [16]; N2: Individuals with multiple lung tumor nodules or tumor in other anatomical regions were omitted [15]; N3: Tumor lesions located centrally and indistinguishable from the surrounding anatomical structures were excluded [16]; N4: PET/CT images of suboptimal quality, deemed inadequate for diagnostic purposes, were not included [14].

According to the final pathological results, the collected data were categorized into positive and negative groups, following established protocols for oncological imaging studies [8,14]. The retrospective study was conducted under a protocol approved by the Institutional Review Board of Vietnam National Cancer Hospital, Hanoi Oncology Hospital and Ho Chi Minh City Oncology Hospital in Vietnam, with patient consent waived as per standard ethical guidelines for retrospective analyses [10]. This approach aligns with common criteria for dataset selection in contemporary PET/CT research [3]. Publicly available PET/CT datasets, spanning from June 2019 to June 2023, were acquired from the aforementioned hospitals. All imaging data were obtained using modern PET/CT scanners, ensuring consistency with international imaging standards [13].

Security and privacy

To protect patient privacy, PET/CT data were anonymized during preprocessing in compliance with international regulations on medical information security, including the General Data Protection Regulation (GDPR) and local ethical standards [2,4]. The dataset was formally approved and licensed for research and machine learning applications by the Institutional Review Boards of the three participating hospitals [10].

Preprocessing and normalization of data

Preprocessing of PET images was performed using Gaussian filtering for noise reduction, followed by attenuation correction and alignment with corresponding CT images, adhering to standardized PET/CT preprocessing protocols [13,17,18]. The data were normalized to ensure uniformity in size and format, rendering them suitable for image segmentation tasks in accordance with international dataset standards [15,16].

Label and annotate

Patients with lung cancer and those without were selected based on medical history findings, following established protocols for oncological imaging studies [8]. Data on patients' age, weight, gender, ^{18}FDG dosage, disease status, smoking history, disease stage, and PET/CT whole-body imaging findings (including tumor location, size, and maximum standardized uptake value—SUVmax) were collected and documented, consistent with standardized data acquisition methods [13].

Based on clinical and medical history, PET/CT imaging results, tumor biopsy findings, and supplementary tests, patients were categorized into two groups: Non-Small Cell Lung Cancer (NSCLC) and other conditions, as described in previous studies [14]. For patients with NSCLC, tumor images were segmented independently by three experts in anatomical and functional imaging, each with at least five years of experience, using 3D-Slicer software, yielding three distinct datasets [15]. These datasets were assessed by nuclear medicine physicians and radiologists. Firstly, PET/CT images were qualitatively evaluated to identify lesions with elevated ^{18}FDG uptake, a technique widely adopted in oncological PET imaging [8]. Subsequently, lesion dimensions were measured, and ^{18}FDG uptake was quantified using SUVmax for primary tumors, lymph nodes, metastases, and other lesions, following standardized quantification protocols [16]. Within the Region of Interest (ROI), SUVmax was determined, delineating two uptake categories: high uptake (SUVmax > 5.0) and moderate uptake (SUVmax 2.5–5.0), consistent with clinical thresholds reported in the literature [14,16].

Tumor volumes were formatted as independent three-dimensional (3D) data matrices to facilitate ML applications. Figures 1 and 2 depict a representative slice of CT and PET images, respectively, with tumor regions segmented by physicians and highlighted for clarity. Figures 3 illustrates a 3D visualization of the tumor volume, with surrounding tissues removed to enhance tumor visibility. These volumes were stored as digital matrices in NRRD format, enabling their use as training data for ML models. This structured formatting, consistent with the dataset's arrangement, supports efficient data processing and aligns with standards for oncological imaging datasets [3,15]. Compared to datasets with 2D segmentation outputs [6,7], this 3D matrix approach enhances spatial analysis for ML, though computational complexity may necessitate optimized algorithms [8].

Fig. 1. Image of a lung tumor marked on a slice from a CT scan.

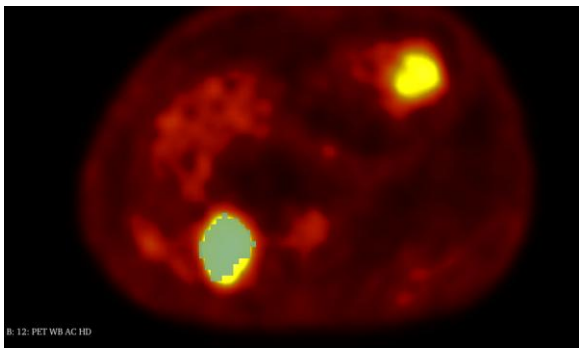

Fig. 2. Image of a lung tumor marked on a slice from a PET scan.

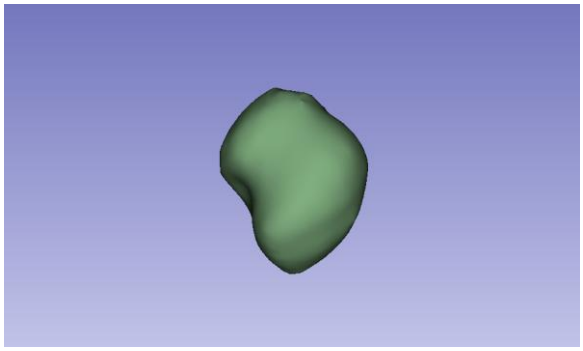

Fig. 3. A three-dimensional image of the tumor volume after removing other surrounding tissue to improve the view of the tumor.

Metric evaluation of the dataset

Consistency and reliability of segmentation labels are critical for PET/CT image segmentation, particularly in determining tumor volume, and require high levels of agreement among physicians in clinical applications [3,8]. In this study, PET/CT image data for each patient were independently segmented by three physicians with expertise in oncological imaging. To assess the similarity between segmented datasets and ensure the quality of segmentation labels, the Relative Volume Difference (RVD) and Dice Similarity Coefficient (DSC) were calculated, following established metrics for evaluating medical image segmentation [15,17].

The RVD was calculated to analyze the volumetric error between automated and manual contour for each tumor, defined as follow Eq. (1) [16]:

$$RVD = \frac{|V_1 - V_2|}{V_1} \times 100\ \% \quad (1)$$

where V_1 and V_2 represent the tumor volumes manually segmented by the first and second physicians, respectively.

The DSC, a widely adopted metric for assessing the overlap between two segmented volumes, was employed to evaluate the agreement between physician pairs or between expert and automated segmentations [2,15]. This metric is expressed by the formula below Eq. (2):

$$DSC = \frac{2 \times |A \cap B|}{|A| + |B|} \quad (2)$$

where A and B denote two segmented volumes, ∩ represents their intersection, and |A|, |B| indicate the sizes of each volume. The DSC ranges from 0 (no overlap) to 1 (perfect overlap), with values of 0.7 to 0.8 typically considered indicative of good segmentation quality for tumor delineation in PET/CT imaging [7,17].

RESULTS AND DISCUSSION

A dataset including 416 PET/CT images was compiled, with 300 images obtained from patients diagnosed with Non-Small Cell Lung Cancer (NSCLC) and the remaining 116 images from individuals without NSCLC. This sample size was deemed statistically sufficient for training and testing machine learning models, surpassing the dataset sizes reported in comparable studies [1,7,8]. The dataset was collected from three major hospitals in Vietnam—Vietnam National Cancer Hospital, Hanoi Oncology Hospital, and Ho Chi Minh City Oncology Hospital—using various modern PET/CT scanners, ensuring diversity in imaging equipment and patient demographics [3]. The cohort included 231 male patients (55.5 %) and 185 female patients (44.5 %), with a mean age of 61.2 ± 9.9 years (range: 25–80 years). No significant age difference was observed between male and female patients ($p > 0.05$), consistent with demographic distributions reported in prior NSCLC studies [14].

Each fused PET/CT image was acquired at a resolution of 512 x 512 pixels, with the PET component at 192 x 192 pixels and the CT component at 512 x 512 pixels, aligning with standard resolutions for PET/CT datasets used in image segmentation [13,17]. The CT images had a pixel size of 1.037 x 1.037 mm² and a slice thickness of 3.26 mm, while the PET images had a pixel size of 3.646 x 3.646 mm² with an identical slice thickness. Hounsfield Unit (HU) values of CT images and Standard Uptake Value (SUV) of PET images varied across a range sufficient to differentiate lung tumour regions from normal tissues, as illustrated in Figs. 4 and 5. These imaging characteristics met the requirements for high-quality datasets suitable for segmentation tasks [15,16].

The PET/CT dataset was structured into two groups based on Non-Small Cell Lung Cancer (NSCLC) status, as illustrated in Fig. 6. For individuals without NSCLC, including healthy subjects and patients with other cancers, data were organized into folders labeled 0BNxxxx, where "0" denotes the absence of NSCLC and "xxxx" represents the individual's code. Each folder contains two NRRD files: "3 CTAC 375mm.nrrd" for CT data and "12 PET WB AC HD.nrrd" for PET data. For NSCLC patients, data were stored in folders labeled 1BNyxxx, with "1" indicating NSCLC, "y" specifying the physician's code (1, 2, or 3) for tumor segmentation, and "xxx" denoting the patient's code. These folders include three NRRD files: "3 CTAC 3.75mm.nrrd" (CT), "12 PET WB AC HD.nrrd" (PET), and "Segmentation.seg.nrrd" (a 3D binary matrix, with 0 for non-tumor and 1 for malignant tumor regions).

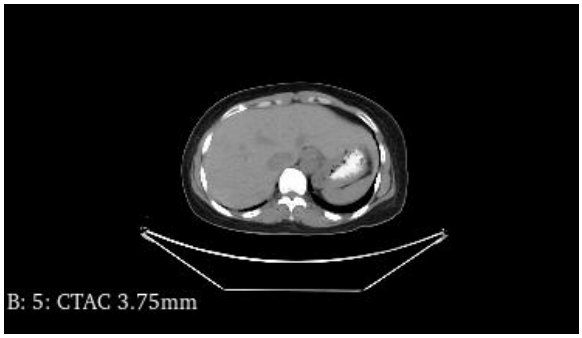

Fig. 4. A slice of a CT image with HU values varying from low to high clearly shows the biological structure of each pixel.

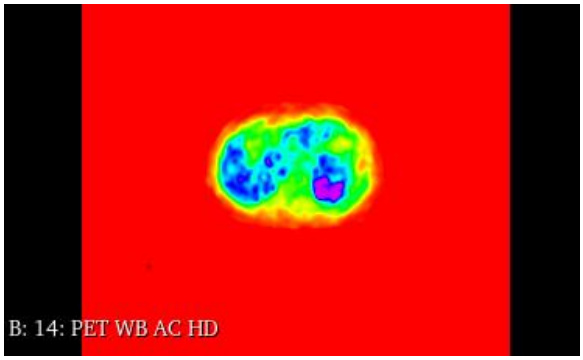

Fig. 5. A slice of a PET image with SUVs varying from low to high clearly shows the biological structure of each pixel.

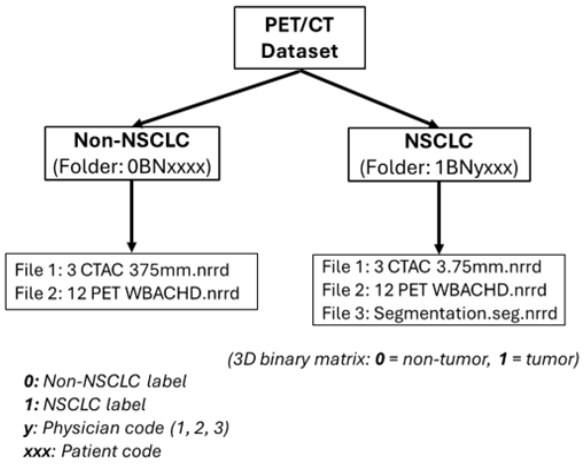

Fig. 6. The flowchart explains how to sort the data into the groups and the order of the file or folder names.

PET and CT images were synchronized and merged with high precision before segmentation, facilitating accurate tumor localization. With clear labeling and consistent file formats, this structured organisation enhances data accessibility for machine learning applications, aligning with standards in similar PET/CT datasets [3,15]. Compared to datasets with less granular physician-specific segmentation [6,7], this approach ensures robust inter-observer validation.

Table 1. Comparison of the relative volume difference of segmentation data between physicians.

Compair between	Range of RVD	Number of patients	Rate (%)
Physican 1st and physican 2sd	0.0-0.1	30	10.0
	0.1-0.2	179	59.6
	0.2-0.3	91	30.4
Physican 2sd and physican 3rd	0.0-0.1	21	7.0
	0.1-0.2	148	49.3
	0.2-0.3	131	43.7
Physican 1st and physican 3rd	0.0-0.1	29	9.7
	0.1-0.2	157	52.3
	0.2-0.3	114	38.0

Table 2. Comparison of dice similarity coefficient of segmentation sets between physicans.

Compair between	Range of DSC	Number of patients	Rate (%)
Physican 1st and physican 2sd	0.9-1.0	32	10.7
	0.8-0.9	183	61.0
	0.7-0.8	85	28.3
Physican 2sd and physican 3rd	0.9-1.0	25	8.3
	0.8-0.9	154	51.4
	0.7-0.8	121	40.3
Physican 1st and physican 3rd	0.9-1.0	34	11.4
	0.8-0.9	169	56.3
	0.7-0.8	97	32.3

Table 3. Statistics on tumor size of non-small cell lung cancer patients.

Size of tumor (cm)	Number of patients	Rate (%)
≤ 3	151	50.33
>3-5	89	29.67
>5-7	60	20.00
X±SD	2.8 ± 1.0 (1.2 – 7.1) cm	

Table 4. Statistics of ^{18}FDG absorption (SUVmax) according to tumor size.

Size of tumor (cm)	Number of patients	SUVmax
≤ 2	53	4.2±1.8
>2-3	98	5.6±2.7
>3-5	89	8.0±3.5
>5-7	60	17.5±12.8
Total	300	5.8 ± 3.5

The Relative Volume Difference (RVD) was calculated to assess volumetric discrepancies between physician-segmented tumor volumes, yielding a mean RVD of 20.0 % (Table 1). This low discrepancy, particularly between the first and second physicians, indicates high inter-observer consistency, comparable to or surpassing values in similar PET/CT studies [3,15].

The Dice similarity coefficient (DSC) was computed to evaluate segmentation overlap, with 100% of patient data achieving a DSC ≥ 0.70 (mean: 0.802; range: 0.70–0.983; Table 2). The highest agreement occurred between the first and second physicians (DSC = 0.823), aligning with acceptable thresholds for tumor segmentation (0.7–0.8) reported in prior research [7,14]. These metrics confirm the dataset's segmentation reliability, establishing it as a good resource for testing machine learning algorithms [8].

Tumor characteristics were analyzed, with sizes ranging from 1.2 to 7.1 cm (mean: 2.8 ± 1.0 cm) and a mean ^{18}FDG uptake (SUVmax) of 5.8 ± 3.5 (Table 3). Tumors in the left lung exhibited slightly higher SUVmax than those in the right lung, though the difference was not significant ($p = 0.21$), contrasting with some studies reporting laterality effects [4]. A moderate positive correlation was observed between SUVmax and tumor size ($r = 0.58$), with SUVmax increasing significantly for larger tumors (mean SUVmax: 8.0 ± 3.5 for 3–5 cm; 5.6 ± 2.7 for 2–3 cm; 2.4–4.2 for < 2 cm; Table 4). These findings align with

prior NSCLC studies noting higher ^{18}FDG uptake in larger tumors [14,16]. Lesions < 1 cm showed low ^{18}FDG uptake, necessitating careful CT evaluation to avoid oversight, consistent with clinical guidelines [16,17]. The dataset's segmentation consistency and tumor characteristics, comparable to high-quality PET/CT datasets [6,7], support its suitability for developing accurate machine learning models. However, inter-scanner variability in SUVmax measurements may require further standardization [5,13].

CONCLUSION

A comprehensive PET/CT dataset for Non-Small Cell Lung Cancer (NSCLC) was established, encompassing 416 images from patients in Vietnam. The dataset includes patient metadata (age, gender, weight, FDG dose, smoking history), labeled DICOM files of PET and CT images, and NRRD files with tumor segmentation data from three independent physicians for 300 NSCLC cases. Each patient's imaging data comprises 200–300 slices, with segmentation metrics demonstrating high reliability (mean Dice similarity coefficient: 0.803; mean relative volume difference: 20.0 %). This dataset's size, diversity, and segmentation quality make it a valuable resource for advancing machine learning applications in NSCLC research. Future efforts should focus on standardizing imaging protocols and validating models across diverse populations to enhance clinical applicability.

ACKNOWLEDGMENT

This work was financially supported by the Vietnamese Ministry of Science and Technology, contract number DTCB.13/22/VKHKTHN.

AUTHOR CONTRIBUTION

Tuan Ho Quang first author and second author, Duong Tran Thuy, equally contributed as the main contributors of this paper. All authors read and approved the final version of the paper.

REFERENCES

1. M. Schwyzer, D. A. Ferraro, U. J. Muehlematter *et al.,* Lung Cancer **126** (2018) 170.
2. I. Domingues, G. Pereira, P. Martins *et al.,* Artif. Intell. Rev. **53** (2020) 4093.
3. B. Foster, U. Bagci, A. Mansoor *et al.,* Comput. Biol. Med. **50** (2014) 76.
4. Y. Guo, Y. Feng, J. Sun *et al.,* Comput. Math. Methods Med. **2014** (2014) 1.
5. H. Wang, Z. Zhou, Y. Li *et al.,* EJNMMI Res. **7** (2017) 1.
6. X. Zhao, L. Li, W. Lu *et al.,* Phys. Med. Biol. **64** (2018) 015011.
7. M. Carles, D. Kuhn, T. Fechter *et al.,* Eur. Radiol. **34** (2024) 6701.
8. P. Blanc-Durand, S. Jégou, S. Kanoun *et al.,* Eur. J. Nucl. Med. Mol. Imaging **48** (2020) 1362.
9. F. Song, X. Song, Y. Feng *et al.,* Med. Phys. **50** (2023) 4351.
10. F. W. Prior, K. Clark, P. Commean *et al., TCIA: An Information Resource to Enable Open Science,* 2013 35th Annual International Conference of the IEEE Engineering in Medicine and Biology Society (EMBC) (2013) 1282.
11. A. P. Reeves and W. J. Kostis, Radiol. Clin. **38** (2000) 497.
12. M. Firmino, A. H. Morais, R. M. Mendoça *et al.,* Biomed. Eng. Online **13** (2014) 1.
13. R. Boellaard, J. Nucl. Med. **50** (2009) 11S.
14. S. P. Primakov, A. Ibrahim, J. E. V. Timmeren *et al.*, Nat. Commun. **13** (2022) 3423.
15. A. Fedorov, R. Beichel, J. Kalpathy-Cramer *et al.,* Magn. Reson. Imaging **30** (2012) 1323.
16. R. L. Wahl, H. Jacene, Y. Kasamon *et al.,* J. Nucl. Med. **50** (2009) 122S.
17. Q. Song, J. Bai, D. Han *et al.,* IEEE Trans. Med. Imaging **32** (2013) 1685.
18. T. Pandiangan, I. Bali and A. R. J. Silalahi, Atom Indones. **45** (2019) 9. (in Indonesian)